Novasinergia
Revista digital de ciencia, ingeniería y tecnología

Unach
UNIVERSIDAD NACIONAL DE CHIMBORAZO

Research article

Machine learning-based classification of push techniques in speed skating

Clasificación basada en aprendizaje automático de técnicas de empuje en patinaje de velocidad

Ximena Albornoz-Tepan[1], Sebastián Ulloa-Montaleza[1], Jorge Barreto[2], Luis I. Minchala[1], Fabian Astudillo-Salinas[1]

[1]*Departamento de Ingeniería Eléctrica, Electrónica y de Telecomunicaciones, Universidad de Cuenca, Cuenca, Ecuador, 010207;*

[2]*Carrera de Pedagogía de la Actividad Física y el Deporte, Universidad de Cuenca, Cuenca, Ecuador, 010203;*

ximena_alb@hotmail.com; bryan.ulloa.cuenca@gmail.com; jorge.barreto@ucuenca.edu.ec; isamel.minchala@ucuenca.edu.ec

*Correspondencia: fabian.astudillos@ucuenca.edu.ec

Citación: Albornoz-Tepan, X.; Ulloa-Montaleza, S.; Barreto, J.; Minchala, L. & Astudillo-Salinas, F., (2026). Machine Learning-Based Classification of Push Techniques in Speed Skating. *Novasinergia. 9*(2). 148-173.

https://doi.org/10.37135/ns.01.18.08

Recibido: 04 marzo 2026
Aceptado: 28 mayo 2026
Publicado: 08 julio 2026

Novasinergia
ISSN: 2631-2654

Abstract: Speed skating is a prestigious sport that requires technical skills and optimal physical condition. During training, computer vision and Machine Learning (ML) techniques can help improve skating performance and biomechanical analysis. However, limited research has addressed the automated classification of speed skating push techniques using pose estimation methods. In this regard, the OpenPose model is used to extract data on the skater's joints and key points for movement analysis and push classification. The classification methodology implied exploring two main approaches. The first approach uses image classification based on Skeleton Gait Energy Images (SGEI) and a Convolutional Neural Network (CNN) with the VGG19 architecture and transfer learning, achieving an accuracy of 90.72%. The second approach uses biomechanical feature vectors through a Support Vector Machine (SVM) system and a Random Forest (RF) algorithm, achieving accuracies of 94% and 92%, respectively. The classification task considered three skating push techniques: classic push, double push, and pendulum push, which are biomechanically relevant due to their influence on propulsion efficiency, balance, and skating performance. Key findings indicate that feature-based models (SVM/RF) achieved higher precision and faster execution, while the CNN approach provided greater flexibility through data augmentation and automated parameter tuning. Furthermore, the "double push" technique was the most accurately classified movement across all evaluated models. The proposed framework contributes to the limited research on automated classification of skating push using pose estimation and ML techniques for biomechanical and sports performance analysis.

Keywords: Biomechanics, Convolutional Neural Network, Machine Learning, OpenPose, Speed skating.

Resumen: *El patinaje de velocidad es un deporte prestigioso que requiere habilidades técnicas y una condición física óptima. Durante el entrenamiento, las técnicas de visión artificial y aprendizaje automático (ML) pueden contribuir a mejorar el rendimiento en el patinaje y el análisis biomecánico. Sin embargo, la investigación sobre la clasificación automatizada de las técnicas de empuje en el patinaje de velocidad mediante métodos de estimación de la postura es limitada. En este sentido, se propone el modelo OpenPose para obtener datos de las articulaciones y puntos clave del patinador para el análisis del movimiento y la clasificación del empuje. La metodología de clasificación implicó explorar dos enfoques principales. El primer enfoque utiliza la clasificación de imágenes mediante imágenes de energía de la marcha del esqueleto (SGEI) y una red neuronal convolucional (CNN) basada en la arquitectura VGG19 con aprendizaje por transferencia, logrando una precisión del 90,72 %. El segundo enfoque utiliza vectores de características biomecánicas mediante un sistema de máquina de vectores de soporte (SVM) y un algoritmo de bosque aleatorio (RF), logrando precisiones del 94 % y el 92 %, respectivamente. La tarea de clasificación consideró tres técnicas de impulso en patinaje: impulso clásico, impulso doble e impulso pendular, las cuales son biomecánicamente relevantes debido a su influencia en la eficiencia de la propulsión, el equilibrio y el rendimiento en patinaje. Los hallazgos clave indican que los modelos basados en características (SVM/RF) lograron mayor precisión y una ejecución más rápida, mientras que el enfoque CNN proporcionó mayor flexibilidad a través del aumento de datos y el ajuste automático de parámetros. Además, la técnica de "impulso doble" fue el movimiento clasificado con mayor precisión en todos los modelos evaluados. El marco propuesto contribuye a la escasa investigación sobre la clasificación automatizada del impulso en patinaje mediante la estimación de la pose y técnicas de aprendizaje automático para el análisis biomecánico y del rendimiento deportivo.*

Palabras clave: *Biomecánica, Red neuronal convolucional, Aprendizaje automático, OpenPose, Patinaje de velocidad.*

1. Introduction

Speed skating is a sport in which mastering a specific technique is crucial for success [1]. Nowadays, multimedia technologies are employed to analyze images and study sports videos to refine athletes' techniques [2]. For instance, the Kinovea software facilitates the analysis of general movement biomechanics by examining videos captured on mobile devices. Recent research, such as the study conducted by [3], has utilized motion capture (MOCAP) technology in conjunction with specialized software capable of interpreting human motion and applying it to biomechanical models. This technology holds significant potential for enhancing skaters' performance and technique. Additionally, it offers an effective way to optimize skaters' training and reduce the risk of injury by focusing on proper posture, movement form, and execution, similar to ergonomic assessment approaches used in sports biomechanics studies. However, it is important to note that this process is time-intensive, as it involves recording multiple video sequences and subsequent manual review [4].

Identifying specific skating techniques manually from video is expert-dependent and can be subject to subjectivity, inconsistency, and fatigue, especially with large datasets. These issues hinder timely, objective feedback from coaches and analysts. Machine learning (ML) offers a more scalable and consistent alternative by automating movement pattern recognition and classification for performance evaluation.

In recent years, there has been a growing body of research exploring the advantages of employing artificial vision techniques and ML in sports [5],[6]. ML enables the analysis of extensive datasets, extracting patterns and features with minimal human intervention. Research in the field of sports has harnessed ML techniques such as Support Vector Machines (SVM) and Convolutional Neural Networks (CNN) to support performance analysis and movement classification. However, limited research has focused on the automated classification of skating push techniques in speed skating using pose estimation and ML approaches.

This research proposes using the OpenPose computer vision system to obtain two-dimensional coordinates of a skater's joints as they move on the track and to classify the type of push they use. The main objective is to evaluate the performance of various ML algorithms to identify and classify three skating push techniques: classic push, double push, and pendulum push from video sequences. These skating techniques present distinct biomechanical characteristics associated with propulsion generation, balance control, movement efficiency, and skating performance. This non-invasive approach allows measurement of various biomechanical parameters and aims to differentiate a skater's skating techniques by detecting patterns and trends during motion. To achieve this, tests and experiments are conducted to assess the system's accuracy and reliability in detecting and classifying skating techniques. A computer vision and artificial intelligence system for skating biomechanics analysis enables precise spatio-temporal parameter extraction and the classification of techniques used by skaters.

In this research, several machine learning techniques are employed for the classification task. Classification algorithms can identify patterns and features in a training dataset and

automatically classify new data into the corresponding categories. A Convolutional Neural Network (CNN) is a neural network architecture composed of multiple convolutional layers that apply convolutions between filters (or kernels) and the input image. Each kernel is a matrix whose dimensions depend on the number of channels in the input image and can extract specific features, such as edges, textures, or shapes [7]. Additionally, there are pooling layers, which reduce the dimensionality of the output from a layer, and dense layers, which are fully connected and are used for final classification. CNNs use an optimization algorithm called Stochastic Gradient Descent (SGD) to adjust the network weights so that the outputs closely approximate the training data labels [8]. VGG19 is a deep convolutional neural network widely used in image classification, consisting of 19 layers, including 16 convolutional layers and three fully connected layers [9].

A Support Vector Machine (SVM) is a supervised learning model used to determine the class or category to which an input data point belongs. Its objective is to find the hyperplane that best separates classes in a high-dimensional space, maximizing the margin between them, thereby classifying new data points based on their position relative to the identified hyperplane [10]. In classification with non-linear data, a kernel function is used to map the data to a feature space, enabling their separation by a hyperplane in a higher-dimensional space [11]. Random Forest (RF) is an ensemble learning method that constructs multiple decision trees during training and outputs the class that is the mode of the individual trees, reducing overfitting and improving generalization.

The main contribution of this study is the comparative evaluation of two different classification paradigms for skating push recognition: a vision-based deep learning approach using SGEI representations with a CNN based on VGG19, and biomechanical feature-based machine learning approaches using RF and SVM classifiers. This comparison provides insights into the advantages, limitations, computational efficiency, and classification performance of both approaches for sports biomechanics analysis.

2. Methodology

This section describes the methodology used to classify push techniques in speed skating. The study follows a structured pipeline consisting of four stages: (1) data acquisition and preprocessing, (2) feature engineering and parameterization, (3) model selection and training, and (4) model validation and performance evaluation. The methodology focuses on two classification approaches: image-based classification using SGEI representations with a CNN, and feature vector-based classification using biomechanical variables with SVM and RF algorithms.

2.1. Data Acquisition and Preprocessing

Speed skating is a sport that relies on lateral and diagonal gliding on skates, where mastering an efficient technique is essential to optimize physical capacity [12],[13],[14]. This research studies the straightway skating technique, which comprises five phases: Basic Position, Push, Takeoff, Recovery, and Regain. Each phase plays a fundamental role in the skating technique and contributes to the smoothness of the movement (Figure 1). Three types of push are identified for classification: (a) the classic push, where the support skate

remains perpendicular to the ground (Figure 2); (b) the pendulum push, where one skate pushes while the opposite skate exerts a pull with an inclination of approximately +/-25 degrees (Figure 3); and (c) the double push, characterized by a constant movement in the supporting leg with a smooth transition between push and pull, shifting the body laterally with an inclination of approximately +/-25 degrees (Figure 4) [15], [16]. These skating push techniques exhibit distinct biomechanical characteristics associated with propulsion generation, balance control, lateral body displacement, and skating efficiency, making them suitable for automated movement classification and biomechanical performance analysis.

a. Types of Push

The push refers to the force a skater exerts against the track's surface to propel themselves along their trajectory. The direction of the push may vary depending on the skater's speed and the slope of the surface [15]. Differences in push execution directly affect skating propulsion, stability, and movement efficiency, making push classification relevant for biomechanical analysis and performance optimization. There are three types of push:

In the classic push (Figure 2), the support skate remains perpendicular to the ground.

Figure 2. Classic push (right cycle)

The pendulum push occurs when one skate pushes, while the opposite skate exerts a pull with an inclination of approximately ±25° (Figure 3).

Figure 3. Pendulum push (right cycle)

During the double push, there is constant movement of the supporting leg, with a smooth transition between push and pull that shifts the body laterally at an inclination of approximately ±25 degrees (Figure 4) [16].

Figure 4. Double push (right cycle)

b. Data Acquisition Protocol

Three mobile cameras are used: two for the sagittal view and one for the frontal view. The rear camera of an iPhone X, at 60 fps and Ultra High Definition (UHD) resolution, is used for the front view. Two identical devices, the Xiaomi Redmi Note 10 Pro, at 240 fps and HD resolution, are employed for the sagittal view. Skateboard videos for this study were captured using smartphones to simplify data collection, preserve the naturalness of athletes' movements, and align with the project's budgetary constraints. While professional digital cameras with advanced subject recognition were initially considered, preliminary testing revealed unsatisfactory performance in real-world skating conditions. In contrast, modern smartphones with high-resolution sensors and image stabilization deliver superior video quality. This practical and cost-effective approach enabled flexible data acquisition without disrupting athletes, and, despite potential limitations in precision compared to high-end vision systems, the image quality afforded by smartphones was deemed sufficient for the goals of this phase.

The video acquisition equipment is mounted on tripods and set to a height of 1.26 meters. The two side cameras are positioned 6.88 meters from the track and 11 meters apart. The front camera is placed 9.32 meters from the section delimited by cones where skaters perform the straight technique. These measurements were defined empirically. The area of the track where the video is captured is delimited by signaling cones to account for the athletes' lateral movement.

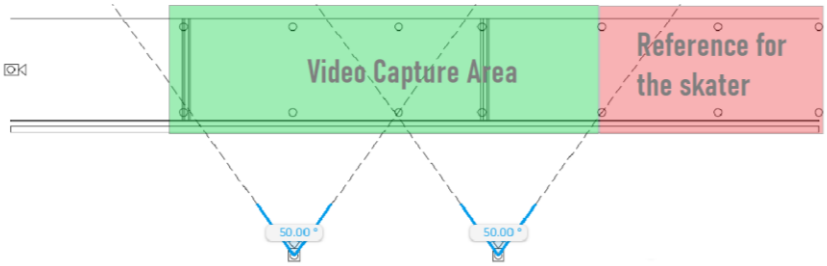

Figure 5. Distribution of cameras and reference marks.

Background music was used to facilitate subsequent video synchronization using audio in Filmora 12. The mentioned software enables precise cuts and consistent merging of different recording angles by using videos that share the same audio.

The participants' ages range from 10 to 24 years, with six male participants and thirteen female skaters. Each athlete performs one of the three possible push techniques during straight-line skating.

c. Data Pre-Processing

The collected data is processed to extract information on joint and extremity movement to classify the type of push a skater uses. This procedure, illustrated in Figure 6, involves feeding the videos to the VGG19/CNN to get an SGEI graph and a set of feature vectors.

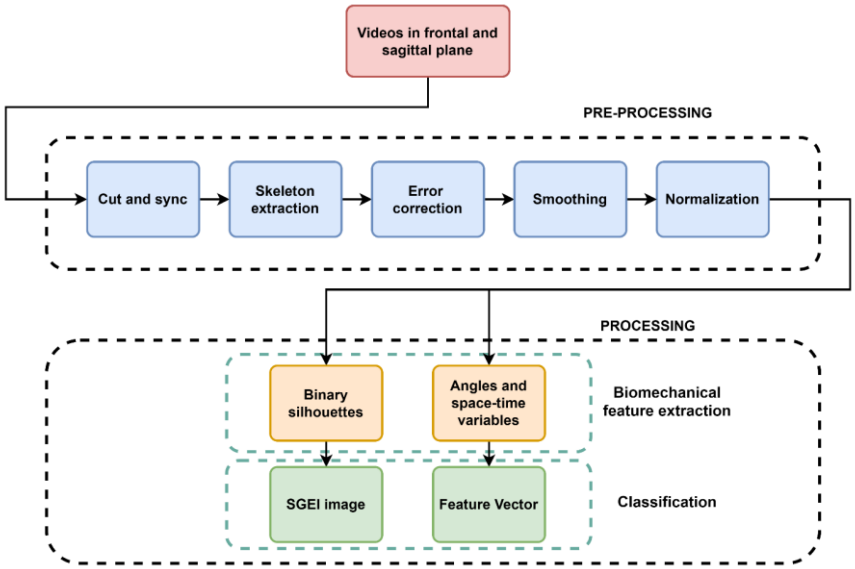

Figure 6. Process scheme.

d. Video Cutting and Synchronization

The videos collected during the data collection process do not have the same duration. Furthermore, they capture information both before and after the execution of the straight-line roller-skating technique. This entails cutting the videos and removing the portions before and after the roller-skating process in the designated area. The synchronization process involves temporally aligning two video sequences so they match in time and play back coherently.

e. Skeleton Extraction

Skeleton extraction is performed using OpenPose, which relies on CNNs to determine its output information. When a video is input to OpenPose, it generates output in both video and JSON formats, providing 2D coordinates (x, y) describing the locations of key points.

f. Error Correction

This stage involves correcting errors in joint coordinate data extracted from JSON outputs generated by OpenPose. Accurate preprocessing at this level ensures the integrity of the kinematic features derived from the data, which directly influences the downstream performance and generalization capability of the classification algorithms. Three main types of errors are identified:

Type 1: Occurs when OpenPose fails to detect a specific keypoint in a frame and assigns a default value of (0, 0).

Type 2: Results from incorrect or noisy coordinate estimations due to motion blur, lighting inconsistencies, or shadows.

Type 3: Involves body part swapping, where coordinates are mistakenly assigned to the opposite side of the body (typically the legs).

To address these issues, the coordinate data are transformed into a time series. Figure 7 shows two such time series of the x-coordinates of the left and right ankles in sagittal view. Each time series is analyzed independently.

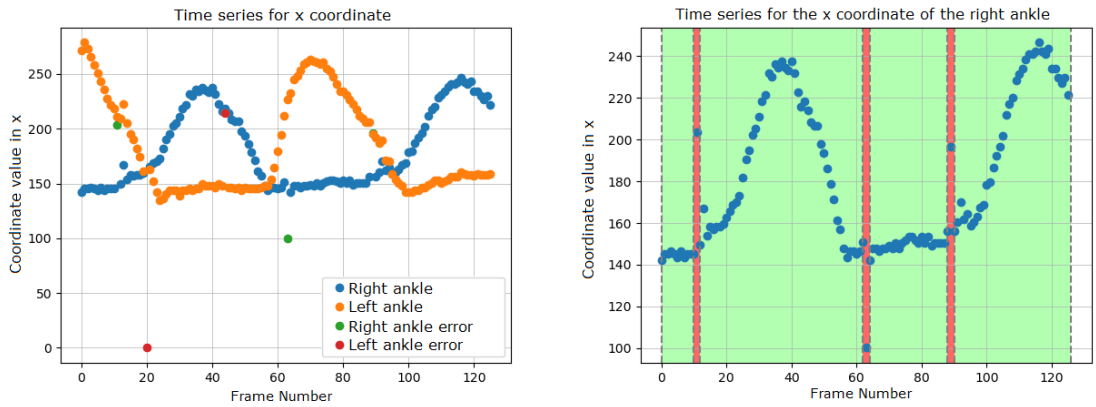

Figure 7. (a) Time series for the x coordinates of the ankle points, Sagittal View. (b) Separation into error-free intervals and intervals with errors.

For Type 1 errors, interpolation is used to estimate realistic values. For other error types, we assess whether a data point deviates significantly from its previous value. Equations (1) and (2) define dynamic thresholds used to flag such deviations:

$$\text{thrup} = \bar{d} + 2 \cdot \text{sd} \quad (1)$$

$$\text{thrdo} = \bar{d} - 2 \cdot \text{sd} \quad (2)$$

where $\bar{d}$ is the mean of the differences between consecutive time-series values, and sd is their standard deviation. A point is flagged as an outlier if the difference from the previous value exceeds the upper threshold thrup, or falls below the lower threshold thrdo. This approach, based on a 2-standard-deviation criterion, captures approximately 95% of values under the assumption of normality and effectively identifies noise and mislabeled data.

To further refine detection, an empirical rule is applied: intervals with fewer than 10 consecutive valid values are classified as error zones, while longer sequences are considered reliable. Once identified, these erroneous segments undergo an iterative smoothing process, illustrated in Figure 8, which improves the consistency of the biomechanical features extracted for subsequent classification.

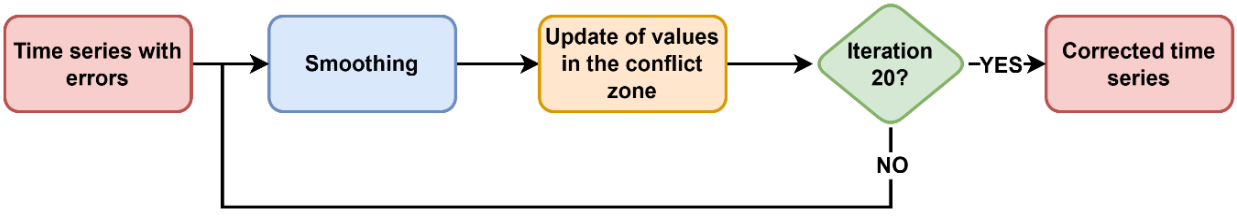

Figure 8. Flowchart for error correction through iterative smoothing.

Smoothing is performed using a discrete Hanning window of size 10 to preserve local trends. The affected regions are replaced with the smoothed values. This is repeated

iteratively, up to a maximum of 20 iterations, or until convergence is achieved. Figure 9 shows the outcome of this process.

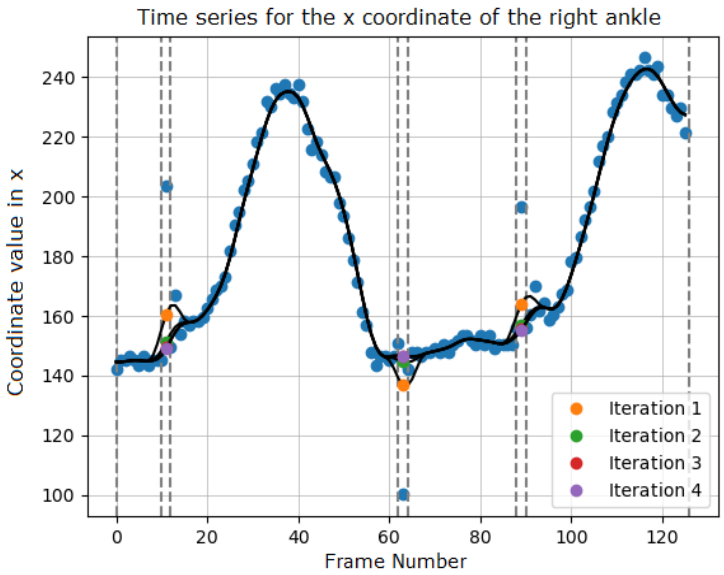

Figure 9. Iterative Smoothing for Error Correction in Time Series.

g. Data Smoothing

To obtain a clearer view of the time series trend, a smoothing process is implemented using a Hanning window. This process involves convolving the time sequence with the window, allowing a more precise representation of the series' behavior.

h. Data Normalization

The smoothed data is normalized to ensure they all fall within a common scale. This process eliminates magnitude disparities among the data, thus facilitating their comprehension and analysis (Figure 10).

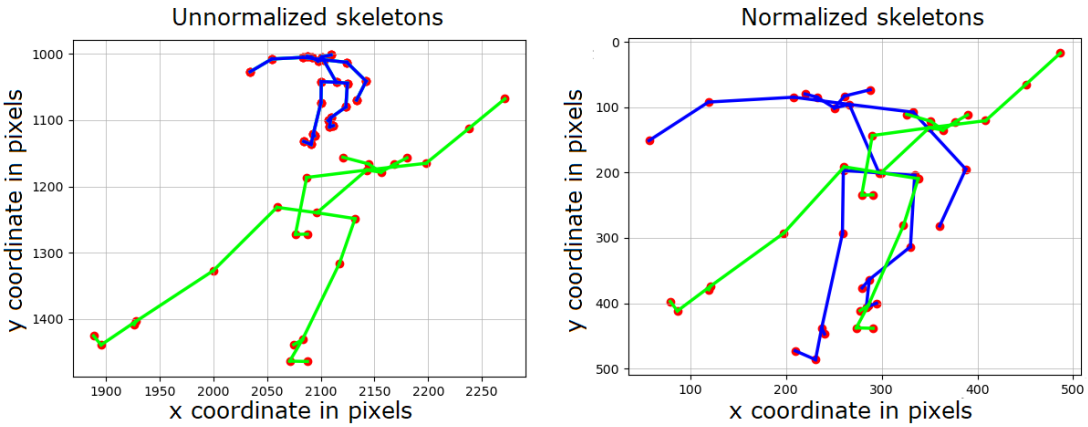

Figure 10. (a) Data from an individual in two different frames without normalization. (b) Data from an individual in two different frames after applying normalization.

2.2. Feature Engineering and Parameterization

a. OpenPose and the Tools for Motion Capture

The MOCAP system enables the transfer of human motion to biomechanical models, both two-dimensional and three-dimensional, through a combination of specialized hardware and software [3].

On the other hand, there is OpenPose, a computer vision system capable of real-time detection and tracking of human bodies through RGB cameras and processing previously recorded images and videos. OpenPose relies on two main components: keypoint confidence maps and Part Affinity Fields (PAFs). Confidence maps indicate the probability of the presence of a keypoint, while PAFs are vector fields that contain information about the orientation and direction between two keypoints [17].

b. Pose Data Normalization

When capturing a person's movement on video, their relative size and position within the frame may vary due to differences in body proportions and camera angles. To ensure that the analysis remains consistent across individuals and recording conditions, a normalization step is applied to the skeletal joint coordinates.

Following the approach proposed in [18], [19], Equation (3) is used to normalize each joint position by centering it around the hip and scaling it with respect to the body height. This allows us to characterize the skeleton independently of its absolute location or size in the image, making it suitable for comparison and classification.

$$j't,i = (xt,i - x\ cm\ t\ ,\ yt,i - y\ cm\ t\ ) / ht(jN\ t\ ,\ jtm\ t\ ) \quad (3)$$

where t denotes the frame number, $j't,i = (xt,i,\ yt,i)$ $(i = 0,\ldots,24)$ represents the normalized coordinates of joint i, cm refers to the hip center, and ht is the Euclidean distance from the nose (jN t) to the midpoint between the left and right ankles (jtm t).

This normalization process is essential to our objective of classifying skating push techniques, as it ensures that joint movement data are expressed on a common scale and are thus directly comparable across different skaters. Reducing inter-subject variability improves the accuracy and generalizability of the machine learning models used in subsequent stages.

c. Gait Energy Image (GEI)

The GEI is a widely used representation that summarizes an individual's movement over a gait cycle by averaging binary silhouettes across time. It effectively captures the overall posture and motion dynamics of the subject, making it valuable for tasks such as person identification and abnormal gait classification.

In our study, the GEI is used to create a structured, low-dimensional visual representation of the skater's movement that serves as input for the CNN-based classification system described in Section Results. By condensing the entire movement into a single image, the

GEI enables the convolutional neural network to learn spatial patterns and distinctive traits associated with different types of push techniques.

The GEI is computed following the formulation proposed in [20], as shown in Equation (4):

$$GEI(x, y) = (1/N) \Sigma t=1 \rightarrow N \, Bt(x, y) \quad (4)$$

where Bt(x, y) represents the binary pixel value at coordinates (x, y) in frame t, and N is the total number of frames in a gait cycle.

A variant called the Skeleton Gait Energy Image (SGEI) is also employed in this work. Unlike the traditional GEI, which uses full-body silhouettes, the SGEI is generated from skeleton silhouettes obtained using OpenPose [21]. This alternative focuses on joint movement and posture, offering a more abstract and flexible representation, particularly well-suited to sports movement classification.

d. Extraction of Biomechanical Features

Extracting biomechanical features involves identifying and quantifying athletes' movement patterns, considering joint angles, velocities, and distances. Two approaches are used to extract biomechanical features: the graphical approach, which uses SGEI images for each skater classified by a CNN, and the data-driven approach, which uses feature vectors and implements a classifier with an SVM.

e. Obtaining the SGEI

Images are generated using SGEI from binary silhouette skeletons obtained for each frame of every video and corresponding person. The SGEI combines and summarizes the athlete's information and movement into a single image, enabling visualization of the distinctive characteristics of each thrust type, as shown in Figure 11. This technique provides a clear, consolidated view of the athlete's movements, effectively highlighting the unique features of different thrust types.

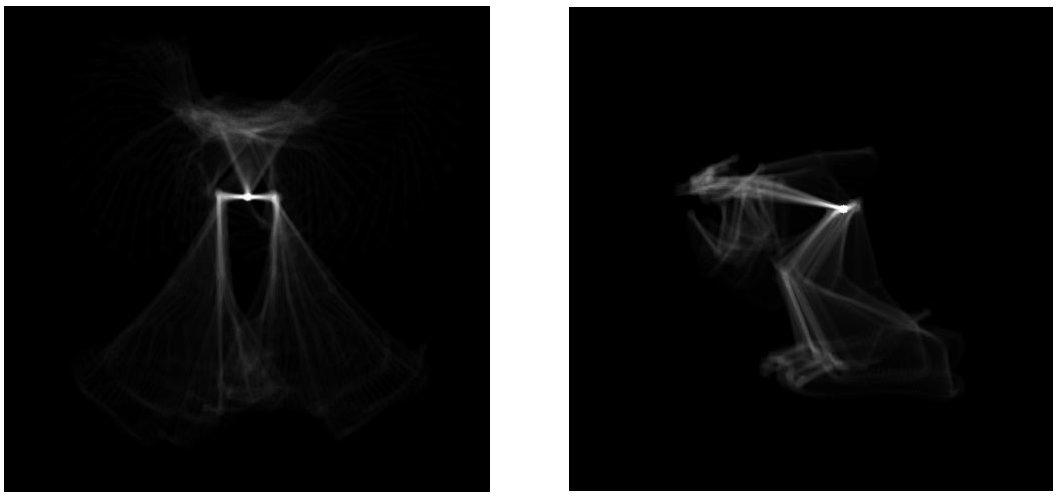

Figure 11. (a) Front view. (b) Sagittal view. SGEI images generated from binary silhouettes.

f. Calculation of Spatio-Temporal Variables and Angles

During the execution of a straight-line thrust, changes and interactions among relevant kinematic variables occur, providing valuable insights. The complete execution, encompassing both the right and left periods, is considered a full cycle. Variables such as distances, times, velocities, and amplitudes are analyzed. Additionally, Table 1 and Figure 12 show the angles corresponding to the frontal and sagittal views. This approach offers a comprehensive examination of motion dynamics, shedding light on the intricate relationships between these kinematic variables.

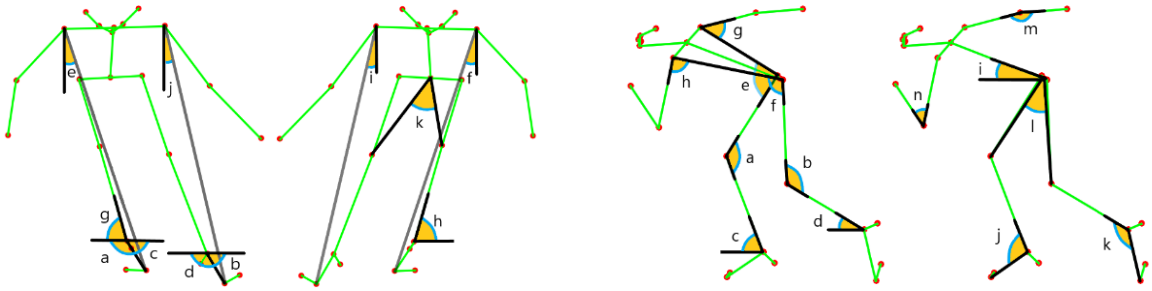

Figure 12. (a) Front view. (b) Sagittal view. Calculated angles.

Table 1. Angles

IDENTIFIER	SAGITTAL	FRONTAL
a	Right knee	Right outside foot
b	Left knee	Left outer foot
c	Right shin	Right inner foot
d	Left shin	Left inner foot
e	Right hip	Right Inner Shoulder Push
f	Left hip	Left Inner Shoulder Push
g	Right shoulder	Right ankle push
h	Left shoulder	Left ankle push
i	Trunk	Right external shoulder push
j	Right ankle	Left external shoulder push
k	Left ankle	Crotch
l	Crotch	–
m	Right elbow	–
n	Left elbow	–

2.3. Model Selection and Training

For the CNN-based approach, a classification model was built using the VGG19 architecture as the foundation and implemented in Python with TensorFlow Keras. Transfer learning was utilized by retaining the pre-trained weights in the initial layers, which detect common patterns, while the subsequent layers adjust their weights based on the skating dataset. Given the limited size of the database, data augmentation techniques were applied

to the input images, including rotation, shifting, and zooming. A Dropout regularization layer was included by randomly deactivating a percentage of neurons during each training epoch to prevent overfitting and improve generalization. The specific hyperparameters of the CNN model are as follows: batch size of 32 to minimize excessive memory usage, SGD optimizer with a learning rate of 0.002, and categorical cross-entropy as the loss function. The VGG19 base model processes 224x224 pixel images through 16 convolutional layers using multiple 3x3 filters, followed by three fully connected layers for final classification.

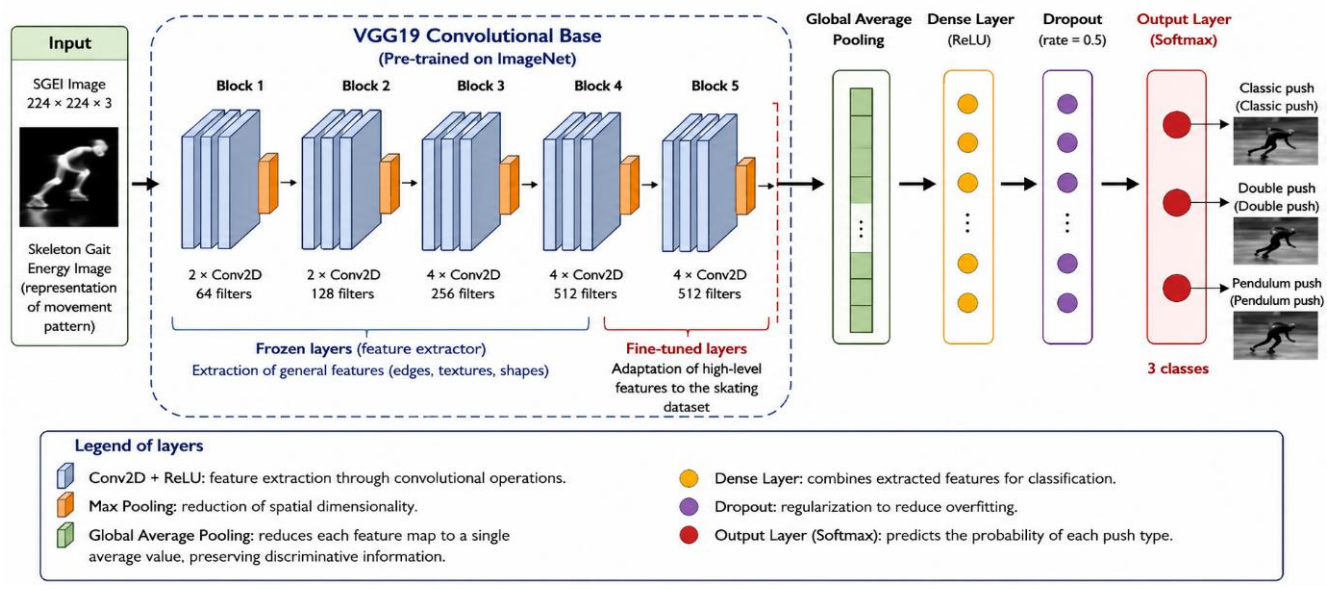

Figure 13. Architecture of the proposed VGG19-based transfer learning model for skating push classification using SGEI representations.

To implement transfer learning, the convolutional base of VGG19 pre-trained on ImageNet was used as a feature extractor. The initial convolutional blocks were frozen to preserve previously learned low-level visual features such as edges, textures, and shapes. The final convolutional block was fine-tuned using the skating dataset to adapt the model to the specific movement patterns present in SGEI images. After the convolutional base, a Global Average Pooling layer, a dense layer with ReLU activation, and a Dropout layer with a rate of 0.5 were added to reduce overfitting and improve generalization. Finally, a Softmax output layer with three neurons was used to classify the skating push techniques: classic push, double push, and pendulum push.

For the SVM-based approach, the feature vectors comprising 95 biomechanical variables were classified using the scikit-learn (sklearn) library. The SVM was configured with a Radial Basis Function (RBF) kernel, selected due to the non-linear nature of the data. The regularization parameter C was set to 0.05, allowing for a wider margin and preventing overfitting, and the gamma parameter was set to 0.004, controlling the influence of each training vector on the construction of the decision hyperplane. These hyperparameter values were selected through iterative search to optimize the balance between model complexity and generalization capability.

For the Random Forest classifier, the same feature vector set was used. The key hyperparameters were configured as follows: n_estimators was set to 100, providing a reasonable balance between computational performance and model precision; the splitting criterion was the Gini impurity index; and a random_state of 1 was set to ensure

reproducibility of the results. No maximum depth constraint was applied, allowing trees to grow until all leaves were pure or contained fewer than the minimum samples required for splitting.

2.4. Model Validation and Performance Metrics

To evaluate the classification performance of the three models, the dataset was partitioned into training, validation, and testing subsets. For the CNN approach, a total of 2,618 SGEI images were divided as follows: 70% for training, 15% for validation, and 15% for testing. This distribution ensures a comprehensive learning and evaluation process, allowing the model to learn from the training set, tune hyperparameters using the validation set, and assess generalization on unseen test data.

For the SVM and RF approaches, a total of 264 feature vectors were processed, with 75% used for training and 25% for testing. To address class imbalance among the three push types (64 classic, 77 double, 123 pendulum), a synthetic data generation process (SMOTE-like oversampling) was applied to the training set, resulting in 240 balanced training vectors per class.

The following performance metrics were used to evaluate all classifiers: (a) overall accuracy, defined as the proportion of correctly classified instances over the total number of instances; (b) confusion matrix, providing a detailed breakdown of true positives, false positives, true negatives, and false negatives for each class; and (c) Receiver Operating Characteristic (ROC) curves with Area Under the Curve (AUC) values, which assess each classifier discriminative ability across varying decision thresholds. Additionally, training accuracy was reported alongside test accuracy to assess potential overfitting, and execution time was measured to compare computational efficiency across classifiers.

3. Results

This section presents the results obtained from the data processing and classification pipeline described in the Methodology. The results are organized in three parts: first, the biomechanical analysis including spatio-temporal parameters and angular measurements; second, the comparative analysis of lower extremity angles across push types; and third, the classification performance evaluation for each machine learning model, including the optimal configurations achieved and the performance metrics obtained on the test sets.

3.1. Biomechanical Analysis

Tables 2, 3, and 4 present the mean and standard deviation (±) of spatio-temporal parameters and angles. The label (D) refers to the right side of the body and (I) to the left side. The results demonstrate a notable similarity to previous skating research conducted by [3] and [16], validating the data obtained through the developed system. Table 2 reveals that the speed of double push (9.34 m/s) exceeds that of the classic push (8.26 m/s) and pendulum push (8.62 m/s). When adjusting distances to a common scale for ease of comparison, time and speed values for different pushes are obtained: classic (1.82 s and 8.06 m/s), double (1.61 s and 9.12 m/s), and pendulum (1.75 s and 8.38 m/s). This confirms that the double push continues to have the shortest time. The double push is more efficient

compared to other types of push, as it achieves higher speed with less effort. This is due to the simultaneous use of both feet and improved movement synchronization, resulting in greater propulsion and speed, indicating more efficient energy use and overall performance.

Table 2. Distances, times, and speeds (average ± standard deviation)

CHARACTERISTICS	CLASSIC	DOUBLE	PENDULUM
Max Lateral Amplitude D (m)	0.5 ± 0.12	0.55 ± 0.12	0.55 ± 0.13
Max Lateral Amplitude I (m)	0.43 ± 0.08	0.45 ± 0.11	0.44 ± 0.10
Half-Cycle Time D (s)	0.75 ± 0.23	0.71 ± 0.22	0.81 ± 0.29
Half-Cycle Time I (s)	0.82 ± 0.30	0.83 ± 0.22	0.90 ± 0.31
Full Cycle Time (s)	1.66 ± 0.62	1.60 ± 0.41	1.75 ± 0.51
Half-Cycle Distance D (m)	6.08 ± 1.56	6.50 ± 1.65	6.76 ± 1.97
Half-Cycle Distance I (m)	6.64 ± 2.17	7.59 ± 1.62	7.51 ± 2.13
Cycle Distance (m)	13.43 ± 4.34	14.57 ± 2.55	14.68 ± 3.27
Speed (m/s)	8.26 ± 0.83	9.34 ± 1.26	8.62 ± 1.09
Max shoulder-to-knee distance D (m)	0.63 ± 0.08	0.63 ± 0.08	0.69 ± 0.07
Max shoulder-to-knee distance I (m)	0.67 ± 0.06	0.72 ± 0.06	0.72 ± 0.06
Min shoulder-to-knee distance D (m)	0.34 ± 0.05	0.36 ± 0.04	0.39 ± 0.04
Min shoulder-to-knee distance I (m)	0.32 ± 0.04	0.37 ± 0.05	0.37 ± 0.05
Max Frontal Amplitude D (m)	0.44 ± 0.09	0.50 ± 0.09	0.49 ± 0.09
Max Frontal Amplitude I (m)	0.39 ± 0.07	0.48 ± 0.10	0.41 ± 0.07
Min Frontal Amplitude D (m)	0.14 ± 0.06	0.11 ± 0.05	0.17 ± 0.05
Min Frontal Amplitude I (m)	0.11 ± 0.08	0.13 ± 0.05	0.17 ± 0.07
Mid-shoulder distance (m)	0.24 ± 0.02	0.27 ± 0.02	0.26 ± 0.02
Max foot-to-ground clearance D (m)	0.19 ± 0.06	0.19 ± 0.05	0.25 ± 0.08
Max foot-to-ground clearance I (m)	0.20 ± 0.06	0.18 ± 0.05	0.26 ± 0.07

Table 3. Mean values of the angles in front view (average ± standard deviation)

CHARACTERISTICS	CLASSIC (°)	DOUBLE (°)	PENDULUM (°)
Outer foot D	84.71 ± 6.53	89.04 ± 4.70	88.91 ± 4.91
Outer foot I	79.56 ± 4.53	82.82 ± 4.63	79.81 ± 5.25
Inner foot D	95.29 ± 6.53	90.96 ± 4.70	91.09 ± 4.91
Inner foot I	100.44 ± 4.53	97.18 ± 4.63	100.19 ± 5.25
Inner Push D	10.71 ± 1.86	12.02 ± 2.03	12.92 ± 2.17
Inner Push I	7.80 ± 1.86	8.99 ± 1.92	9.57 ± 2.40
Outer Push D	18.72 ± 2.47	19.20 ± 1.74	20.31 ± 3.17
Outer Push I	17.03 ± 2.50	19.71 ± 1.62	19.49 ± 2.69
Ankle D	80.36 ± 4.27	82.04 ± 3.32	78.88 ± 4.79
Ankle I	81.51 ± 4.22	84.15 ± 3.11	81.74 ± 4.40
Groin	47.57 ± 6.24	46.58 ± 5.88	48.49 ± 5.85

In Table 3, the average angles of the outer foot for the right (D) (89.04°) and left (I) (82.82°) indicate a greater inclination in the double push, with a more pronounced angle than other push types. The angles for internal (D at 12.92° and I at 9.57°) and external (D at 20.31° and I at 19.49°) pushes illustrate the distinct, non-simultaneous traction and push characteristics of the pendulum push. Table 4 shows that double push involves simultaneous traction and push, thereby reducing the need for excessive knee bending, with average knee angles of right (D) (118.66°) and left (I) (120.3°). However, this type of push requires greater trunk flexion (17.87°) than the classic and pendulum pushes.

Table 4. Mean values of the angles in sagittal view (average ± standard deviation)

CHARACTERISTICS	CLASSIC (°)	DOUBLE (°)	PENDULUM (°)
Trunk	21.25 ± 4.19	17.87 ± 2.74	23.45 ± 4.64
Hip D	86.63 ± 4.52	80.13 ± 3.93	87.42 ± 6.30
Hip I	83.65 ± 6.24	81.15 ± 5.45	85.09 ± 8.73
Knee D	119.01 ± 7.10	118.66 ± 4.42	116.19 ± 7.31
Knee I	118.18 ± 5.71	120.30 ± 5.72	116.33 ± 6.53
Ankle D	102.23 ± 8.62	101.20 ± 4.05	99.88 ± 5.84
Ankle I	97.58 ± 5.06	101.10 ± 4.59	98.35 ± 6.41
Shin D	53.80 ± 6.90	57.74 ± 3.13	52.25 ± 4.99
Shin I	54.85 ± 5.90	55.65 ± 6.09	54.14 ± 6.78
Groin	31.29 ± 7.46	31.18 ± 6.91	33.10 ± 7.34
Elbow D	125.94 ± 18.84	132.01 ± 17.05	116.27 ± 25.44
Elbow I	141.96 ± 14.82	129.60 ± 21.50	141.20 ± 14.75
Shoulder D	51.57 ± 12.15	41.24 ± 15.23	53.07 ± 17.62
Shoulder I	33.83 ± 10.14	27.80 ± 12.82	25.17 ± 17.43

These findings reveal bilateral concordance between the right and left half-cycles, as values on the right side of the body do not differ significantly from those on the left. This indicates a suitable biomechanical balance in the execution of the analyzed movements, as well as an equitable distribution of weight and movement across the lower and upper limbs on both sides of the body. However, it is important to note that results can vary significantly based on the participants' height, weight, flexibility, strength, and coordination. Each individual is unique, and what benefits one person may not necessarily apply to another, depending on their personal characteristics. This observation underscores the importance of considering individual differences when analyzing movement efficiency and effectiveness.

3.2. Comparison of the Angles of the Lower Extremities

Graphs showing the angle as a function of the speed skating cycle are generated, based on the angles of the trunk flexion, knee, and ankle in the sagittal view. The colored regions illustrate the angle variations of the 19 volunteer athletes, while the dark lines represent the average. The red graphs correspond to the classic push, the green graphs denote the double push, and finally, the blue graphs represent the pendulum push. These visual representations provide a clear, detailed comparison of the biomechanical dynamics

of each push technique, highlighting the distinct movement patterns athletes use in speed skating.

The patterns among the different types of pushes are quite similar; however, there are differences in the flexion range at various parts of the cycle. Figure 14 illustrates that during the recovery phase, which spans from 40% to 80% of the cycle, there is a greater trunk flexion. This increased flexion is due to the weight transfer during the push phase. While in the classic push, the recovery phase occupies 42% of the cycle, the pendulum push exhibits less-defined values and a wider range of trunk movement.

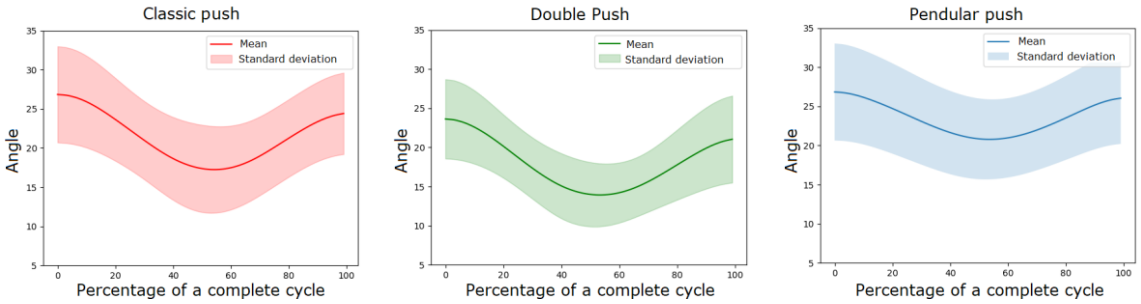

Figure 14. Trunk flexion: (a) Classic push. (b) Double push. (c) Pendulum push.

Figure 15 shows the patterns in the angles of the knee joint of the left leg. Flexion is observed during the push phase, which occurs at 20% of the cycle, meaning a decrease in the angle. At this point, the majority of body weight is supported by the left leg, resulting in maximum flexion during the recovery phase, which occurs from 25% to 80% of the cycle. The final 20% corresponds to the final phase, in which the leg returns to its initial support state. It is noted that in the classic and pendulum pushes, there is greater knee flexion compared to the double push.

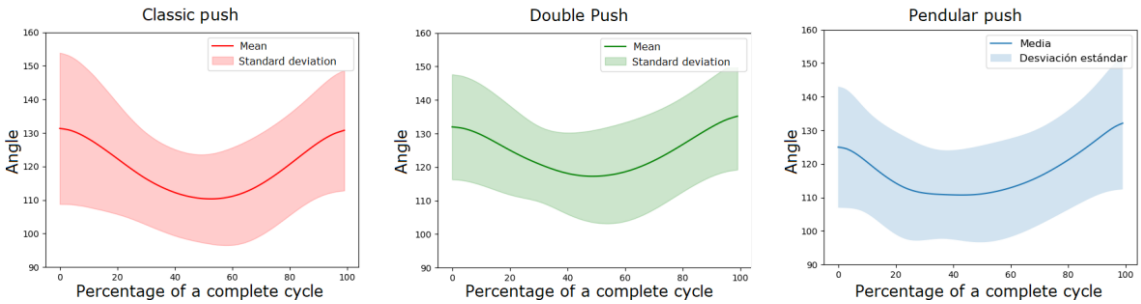

Figure 15. Left knee flexion: (a) Classic push. (b) Double push. (c) Pendulum push.

Figure 16 illustrates the pattern formed by the angle of the right ankle. A more defined pattern is observed in the double push, characterized by a more consistent standard deviation, attributable to its steady incline movement. On the contrary, the classic push exhibits a flattened flexion, reaching a maximum of 125 degrees. In contrast, the pendulum push exhibits a pattern that combines features of both the classic and double pushes.

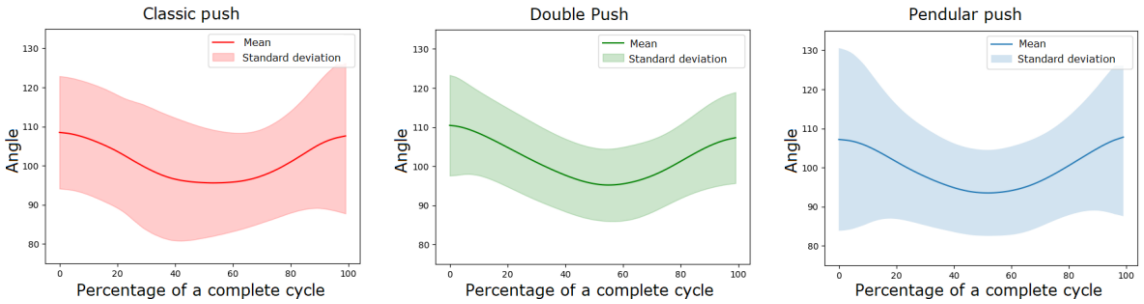

Figure 16. Right ankle flexion: (a) Classic push. (b) Double push. (c) Pendulum push.

3.3. Classification Performance Evaluation

This section presents the classification results for each of the three machine learning approaches evaluated: CNN, SVM, and RF. Each subsection reports the data allocation strategy, optimal hyperparameter configurations, and final performance metrics achieved on the respective test sets. The three push types are numerically identified as classic (0), double (1), and pendulum (2).

a. Classification Using CNN

A total of 2618 Silhouette-based Gait Energy Images (SGEI) were used as input for classification, which was conducted manually by an expert. These images were categorized into 759 classic push, 963 double push, and 896 pendulum push images. For each push type, 70% of the images were assigned to training, 15% to validation, and the remaining 15% to testing. This distribution ensures a comprehensive learning and evaluation process, allowing the models to effectively learn from and adapt to the varied characteristics of each push type.

A batch size of 32 was chosen to minimize excessive memory usage. The model employs an SGD optimizer with a learning rate of 0.002. Additionally, the categorical cross-entropy loss function was used. The CNN-based classification achieved 80.97% accuracy on the training set and 88.92% on the validation set. For testing, 377 Silhouette-based Gait Energy Images (SGEI) were used, including 91 classic push images, 143 double push, and 143 pendulum push images. The results of the confusion matrix and Receiver Operating Characteristic (ROC) curves are presented in Figure 17, which showcase an accuracy of 90.72% and an area under the curve of 98.24%.

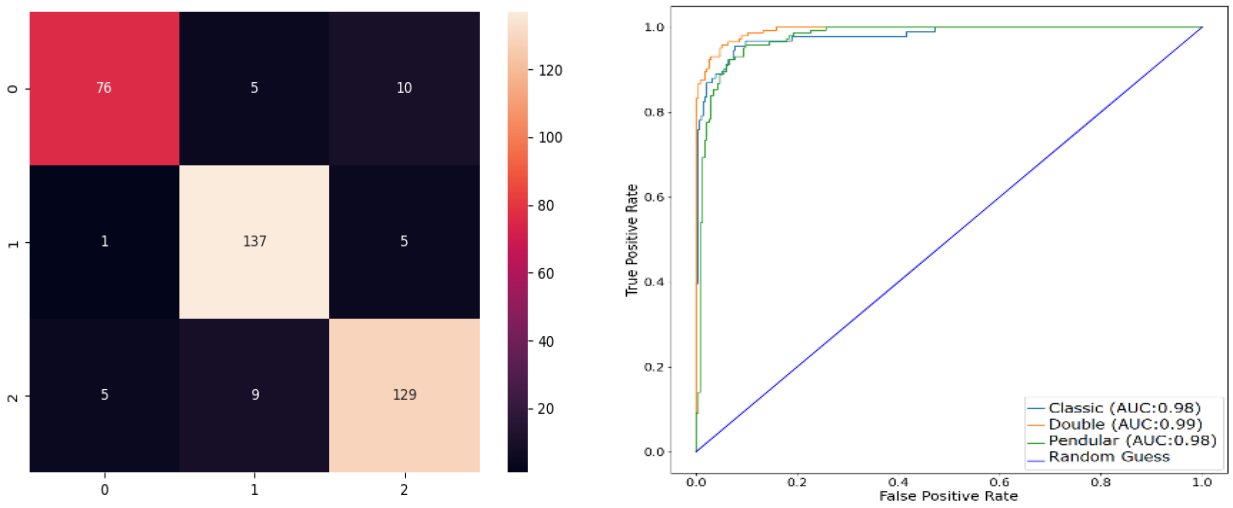

Figure 17. CNN evaluation: (a) Confusion matrix. (b) ROC curve.

b. Classification Using SVM

The feature vector set is classified using the SVM method with an RBF kernel, selected due to the non-linear nature of the data. The C parameter is set to 0.05, allowing for a wider margin, and the Gamma parameter is adjusted to 0.004, thus increasing the influence of each training vector on the construction of the decision hyperplane. This configuration is carefully chosen to balance the model's complexity with the specificity required to accurately classify the non-linear dataset, thereby optimizing the SVM classifier's performance.

A total of 264 feature vectors were processed: 64 corresponding to the classic push class, 77 to the double push class, and 123 to the pendulum push class. These data were divided into a training set comprising 75% of the total and a testing set comprising the remaining 25%. A synthetic data generation process was applied, yielding 240 training vectors per class. An accuracy of 92.22% was achieved on the training data and 93.94% on the test set.

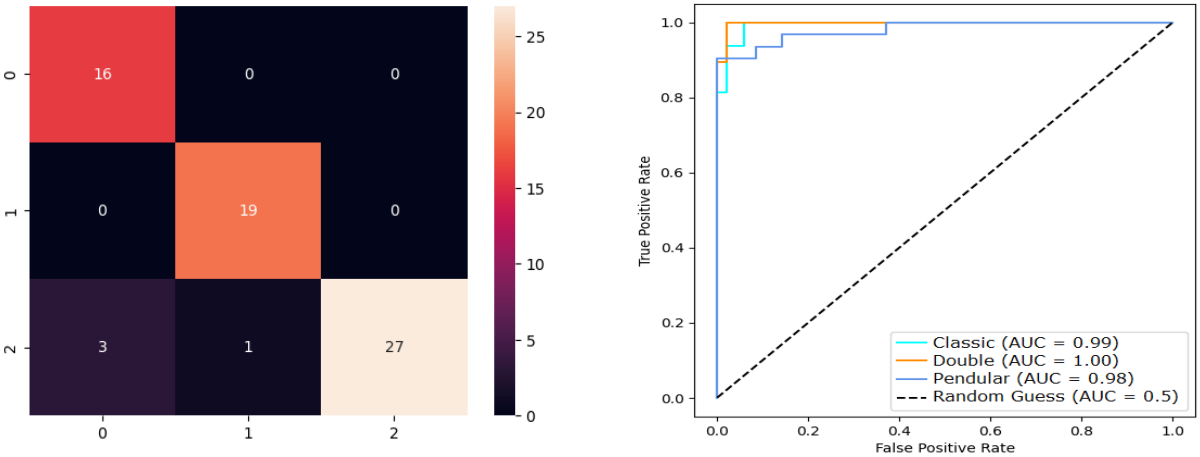

Figure 18. SVM evaluation: (a) Confusion matrix. (b) ROC curve.

c. Classification Using Random Forest

Using the same training and testing sets as for the Support Vector Machine (SVM), an accuracy of 100% was achieved on the training set and 92.42% on the testing set, suggesting potential overfitting of the classifier. Figure 19(b) reveals that the curve for the pendulum class is not as convex as that for the other two classes, which may indicate problems with class imbalance. This observation points to the classifier's high proficiency on the training data, while also highlighting the need for caution regarding its generalization to unseen data, particularly in effectively managing class imbalance.

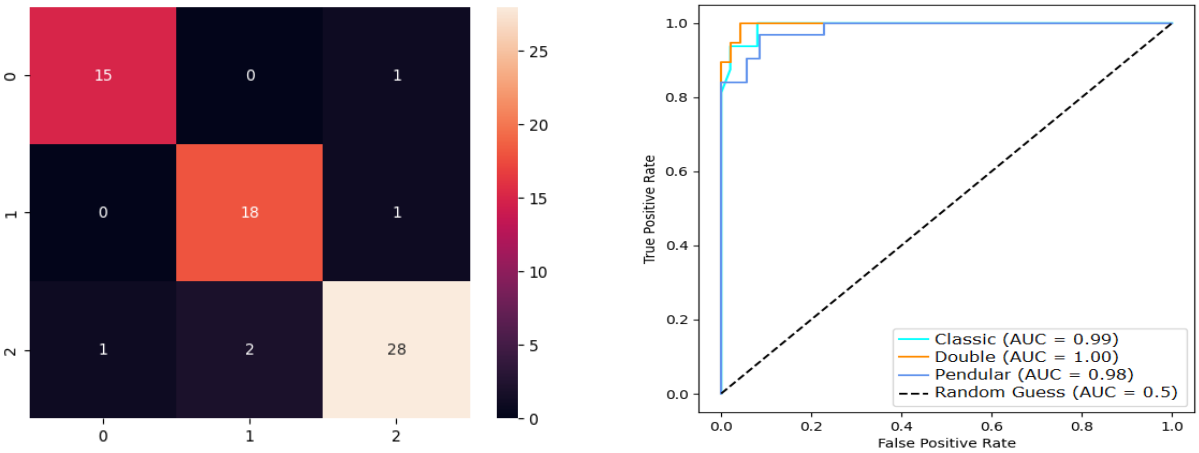

Figure 19. Random Forest evaluation: (a) Confusion matrix. (b) ROC curve.

4. Discussion

The three classification systems presented in this study demonstrate high accuracy on their respective test sets: 90.72% for CNN, 93.94% for SVM, and 92.42% for RF. The confusion matrices and ROC curves indicate promising results for classifying skater push types during the straight-line technique. These results position our work competitively within the growing body of literature on machine learning applications for sports movement analysis and biomechanical classification.

Our SVM-based approach, achieving 93.94% test accuracy with an RBF kernel (C=0.05, gamma=0.004), is consistent with findings reported in related domains. For instance, the integration of OpenPose with SVM for postural analysis in young adults and achieved high classification accuracy using temporal and spatial regression features [22]. Similarly, in combat sports, SVM-based classification of Taekwondo kick types using accelerometer data archieved accuracies exceeding 96% [23]. While our accuracy is slightly lower, this is likely attributable to the higher complexity of skating push classification, which involves subtle differences in body inclination and timing rather than distinctly different movement patterns. The use of smartphone-based video capture, while offering practical advantages in accessibility and cost, introduces additional noise compared to dedicated motion capture systems or wearable inertial sensors.

The CNN approach, using VGG19 transfer learning with SGEI inputs achieved 90.72% accuracy, which aligning with results from similar image-based classification systems in sports. A comprehensive review of pose estimation models and found that OpenPose-based

approaches in sports applications generally achieve accuracy levels above 85% when combined with appropriate deep learning classifiers [24]. Similary, the application of OpenPose for pose estimation in hurdles athletics demonstrated sufficient accuracy for practical athlete development applications [25]. The relatively lower CNN accuracy compared to SVM may be explained by the limited dataset size (2,618 images), as deep learning models typically require larger datasets to fully exploit their capacity for learning complex visual features.

The RF classifier achieved 100% training accuracy but 92.42% test accuracy, suggesting potential overfitting despite its overall strong performance. This pattern is consistent with observations from comparative studies of SVM, RF, KNN, and Logistic Regression for gait classification, which found that ensemble methods tend to overfit when applied to relatively small datasets [26]. The class imbalance in our feature vector dataset (64 classic, 77 double, 123 pendulum vectors) may have contributed to the RF overfitting tendency, even after applying synthetic data generation. Future work should explore more sophisticated class balancing strategies, such as SMOTE with Tomek links or cost-sensitive learning approaches.

The biomechanical analysis results are consistent with prior skating research [3], [16], thereby validating the data obtained through the developed system. The finding that double push achieves a higher speed (9.34 m/s) than classic push (8.26 m/s) and pendulum push (8.62 m/s) aligns with established biomechanical principles, as the double push leverages the simultaneous use of both feet for greater propulsion efficiency. The higher classification performance observed for the “double push” technique may be associated with its more distinctive biomechanical movement pattern, characterized by continuous lateral displacement and smoother transitions between push and pull phases. In contrast, the “classic push” and “pendulum push” present more similar movement characteristics, which may increase classification complexity. Two-dimensional video-based pose estimation has been shown to reliably capture gait parameters comparable to marker-based systems [27], supporting the validity of our OpenPose-based approach for extracting meaningful biomechanical features from video data.

The use of smartphone cameras for data acquisition represents a significant practical advantage of our approach. A similar framework that utilizes smartphone monocular videos for gait analysis and demonstrated that this cost-effective alternative can provide reliable kinematic measurements [28]. Furthermore, the feasibility of using OpenPose for markerless motion analysis in real athletics competitions han been demonstrated, confirming that markerless pose estimation from standard video can be practically deployed in field settings [29]. Our results extend these findings to the specific domain of speed skating technique classification.

The feature vector approach with 95 biomechanical variables outperformed the image-based CNN approach, suggesting that domain-specific feature engineering retains significant value even in the era of deep learning. Among the evaluated models, the SVM classifier achieved the best overall performance, obtaining the highest test accuracy (93.94%) and the shortest execution time, suggesting that biomechanical feature-based approaches are highly effective for skating push classification. This observation is supported by findings indicating that bridging the lab-to-field gap in sports biomechanics often requires careful

integration of domain knowledge with machine learning techniques [30]. Similarly, wearable biomechanical analytics combined with machine learning can enhance sports performance monitoring when appropriate feature selection is applied [31]. The 95-variable feature set used in our study captures joint angles, velocities, and spatio-temporal parameters that directly encode the biomechanical differences between push types.

When comparing computational efficiency, SVM demonstrated significantly shorter execution time (0.692 s) compared to CNN (173.689 s) and RF (2.349 s). This is consistent with the computational characteristics of these algorithms: SVMs with kernel functions are generally efficient for moderately dimensional feature vectors, whereas CNNs require substantial computational resources for image processing during training. The practical implications are important for potential real-time deployment; the SVM classifier combined with a pre-trained OpenPose model could feasibly be deployed for near-real-time feedback during training sessions, as suggested by recent work on edge-computing wearables for sports analytics [32],[33].

Several studies have applied deep learning to related sports analysis tasks with comparable or higher accuracy. The effectiveness of Gait Energy Images for human gait analysis has been demonstrated [20], and skeleton-based GEI representations have been shown to achieve strong classification performance for pathological gait detection [21]. Our adaptation of SGEI for skating push classification extends these approaches to a novel application domain. Additionally, robust classification of baseball player behavior using LSTM networks with multimodal features has been achieved [18], suggesting that temporal sequence models could improve upon our results by capturing the dynamic evolution of skating movements across frames.

Recent reviews have highlighted the growing importance of AI in sports biomechanics. A scoping review spanning 73 studies (2015-2024) found that methodological sophistication has evolved from traditional ML to deep learning architectures that integrate multimodal data [34]. A systematic review of ML for sport-specific movement recognition identified that SVM and RF remain among the most effective traditional approaches for classification tasks with engineered features [35]. Our study contributes to this body of work by demonstrating that these traditional approaches, when combined with computer vision-based feature extraction via OpenPose, can achieve competitive results in a previously unexplored application domain.

The present study has several limitations that should be acknowledged. First, the dataset comprises 19 participants aged 10-24 years, which, while sufficient for the classification task demonstrated, limits the statistical power and generalizability of the findings. Second, using 2D pose estimation from monocular video introduces inherent depth ambiguity, particularly for out-of-plane movements. Accuracy limitations of markerless motion capture for measuring running kinematics have been documented [36], and similar limitations may apply to skating analysis. Third, the hyperparameter optimization was performed through iterative manual search rather than systematic grid search or Bayesian optimization, which may have resulted in suboptimal configurations. Fourth, the absence of k-fold cross-validation limits the robustness assessment of the reported accuracy metrics.

Despite these limitations, this study offers several novel contributions. First, it represents one of the earliest applications of combined computer vision and machine learning to

classify push techniques in speed skating, addressing a gap identified in the sports biomechanics literature. Second, it demonstrates that a non-invasive, smartphone-based approach can yield reliable biomechanical parameters and accurate technique classification, making advanced biomechanical analysis accessible to coaches and athletes without expensive equipment. Third, the comparison of image-based (CNN) and feature-based (SVM, RF) approaches provides practical guidance for selecting classification strategies based on available data and computational resources. In particular, the comparative analysis between the vision-based CNN approach and the biomechanical feature-based ML approaches highlights differences in classification performance, computational efficiency, and feature-extraction capabilities for sports biomechanical analysis. Future work should focus on expanding the dataset, implementing systematic hyperparameter optimization with cross-validation, exploring temporal sequence models such as LSTM or Transformer architectures, and validating the system in real-time training scenarios [37],[38],[39].

5. Conclusions

This study demonstrates the feasibility of extracting and processing video data to obtain Silhouette-based Gait Energy Images (SBGEI) and feature vectors. These elements have been used to develop training, validation, and testing datasets for machine learning (ML)-based classification methods of push types in speed skating. The performance metrics achieved are consistent with findings from similar research efforts demonstrating the effectiveness of these methods for classifying speed skating techniques. This approach not only underscores the utility of video analysis in sports science but also highlights the potential of ML applications to improve our understanding and analysis of athletic performance.

A study has been conducted on biomechanical models of the straight-line skating technique. The distinctive characteristics of the classic push, double push, and pendulum push in skating have been identified, and the main phases of movement during their execution have been described. This investigation not only elucidates the intricate mechanics of skating techniques but also provides a foundational understanding to optimize performance through biomechanical analysis.

OpenPose offers a non-invasive approach for generating dynamic variables relevant to the study, allowing athletes to perform their techniques without relying on devices that restrict their mobility. In addition, skateboard videos were captured using smartphones, eliminating the need for complex or expensive equipment. This method not only facilitates data collection but also ensures that athletes can maintain natural movement patterns, providing authentic insights into athletic performance.

In this study, two classification approaches were explored: SGEI using a CNN, achieving an accuracy of 90.72% with the VGG19 architecture as the foundation, and the feature vector approach with 95 variables derived from a biomechanical analysis using an SVM, achieving an accuracy of 93.94%, and the RF algorithm, achieving an accuracy of 92.42%. These methods demonstrate the potential to combine advanced image processing with biomechanical insights to precisely classify athletic movements.

Our study innovatively uses everyday smartphone video and machine learning to effectively classify speed skating push techniques through Silhouette-based Gait Energy

Images and movement data. Achieving high accuracy with common algorithms confirms the power of these methods for performance analysis. Crucially, our biomechanical modeling reveals key, practical differences between push styles using accessible tools like smartphones and OpenPose, without disturbing athletes. This offers new, real-world insights for optimizing training and understanding technique in speed skating.

Future work will focus on expanding the dataset to include a greater variety of athletes and skating conditions to improve the models' generalizability. Additionally, future studies could explore the classification of other technical maneuvers, such as cornering or starts, to provide a more comprehensive analysis of speed skating performance.

Author Contributions

Conceptualization, X.A.-T. and F.A.-S.; methodology, X.A.-T. and S.U.-M.; software, X.A.-T. and S.U.-M.; validation, X.A.-T., S.U.-M., J.B., L.I.M., and F.A.-S.; formal analysis, X.A.-T.; investigation, X.A.-T. and S.U.-M.; resources, F.A.-S.; data curation, X.A.-T.; writing—original draft preparation, X.A.-T. and S.U.-M.; writing—review and editing, J.B., L.I.M., and F.A.-S.; visualization, X.A.-T.; supervision, F.A.-S.; project administration, F.A.-S. All authors have read and approved the published version of the manuscript.

Acknowledgments

We would like to express our sincere gratitude to the Gabriela Cavalieri Club for their invaluable collaboration in making this work possible. Their commitment and enthusiasm were crucial for the success of this project. Special thanks go to the talented athletes of the club, whose stories and experiences greatly enriched our work.

The Club's support extended beyond the participation of its athletes. We also want to highlight the assistance received from the coaches, parents, and club members, who were always available to help with anything needed.

Furthermore, we extend our heartfelt appreciation to the Ecuadorian Corporation for the Development of Research and Academia (CEDIA) for granting us access to its High-Performance Computing (HPC) cluster. Their support has been instrumental in the development and completion of this project, enabling us to perform complex calculations and large-scale data analysis efficiently. Access to CEDIA's HPC has provided an advanced technological infrastructure indispensable to our research. We also appreciate the technical team at CEDIA for their continuous assistance and support, which ensures optimal utilization of these resources. This project would not have been possible without the collaboration and generosity of CEDIA, and we highly value their commitment to advance research and academia in Ecuador.

Conflict of Interest

The authors report no conflicts of interest related to this research.

Generative Artificial Intelligence (AI) Use Statement

No generative artificial intelligence was used in the preparation of this article.

Funding Sources

This research was funded by the University of Cuenca and CEDIA (Ecuadorian Corporation for the Development of Research and Academia).

References

[1] A. J. Leemreize, "Assessment of performance in speed skating using IMUs," Master's thesis, *Univ. of Twente*, Enschede, Netherlands, 2024. [Online]. Available: https://essay.utwente.nl/fileshare/file/104719/Leemreize_MA_TNW.pdf

[2] P. Madeleine, A. Samani, M. De Zee, and U. Kersting, "Biomechanics of human movement," *IFMBE Proc.*, vol. 34, pp. 237–240, 2011, doi: 10.1007/978-3-642-21683-1_60.

[3] J. Acero, "MÉTODO MOCAP SPORTECH- II&SB PARA LA EVALUACIÓN BIOMECÁNICA DE LA TÉCNICA DEPORTIVA," in *Mem. X Encuentro Internacional en Ciencias de la Actividad Física y del Deporte,* 2026, pp. 9–10. [Online]. Available: https://www.unipamplona.edu.co/unipamplona/portalIG/home_145/recursos/general/14042026/xencuentropamplona2025.pdf

[4] I. Takeda, A. Yamada, and H. Onodera, "Artificial Intelligence-Assisted motion capture for medical applications: a comparative study between markerless and passive marker motion capture," *Comput. Methods Biomech. Biomed. Eng.*, vol. 24, no. 8, pp. 864–873, 2021, doi: 10.1080/10255842.2020.1856372.

[5] Y. Yao, J. Wang, Y. Lai, and L. C. Chen, "Aging Decline in Basketball Career Trend Prediction Based on Machine Learning and LSTM Model," *arXiv preprint arXiv:2509.25858*, 2025, doi: 10.48550/arXiv.2509.25858.

[6] Z. Lu and X. Mao, "A gait recognition method based on deep learning and attention transformer," in *Fourth International Conference on Signal Processing and Computer Science (SPCS 2023)*, vol. 12970, 2023, doi: 10.1117/12.3012246.

[7] H. H. Aghdam and E. J. Heravi, *Guide to convolutional neural networks*, Springer International Publishing, 2017. doi: 10.1007/978-3-319-57550-6.

[8] R. Venkatesan and B. Li, *Convolutional neural networks in visual computing: A concise guide*. Boca Raton, FL, USA: CRC Press, 2017.

[9] M. Bansal, M. Kumar, M. Sachdeva, and A. Mittal, "Transfer learning for image classification using VGG19: Caltech-101 image data set," *J. Ambient Intell. Humaniz. Comput.*, vol. 14, no. 4, pp. 3609-3620, sep. 2021, doi: 10.1007/s12652-021-03488-.

[10] J. A. Carter, A. R. Rivadulla, and E. Preatoni, "A support vector machine algorithm can successfully classify running ability when trained with wearable sensor data from anatomical locations typical of consumer technology," *Sport. Biomech.*, vol. 23, no. 11, pp. 2372–2389, jan. 2022, doi: 10.1080/14763141.2022.2027509.

[11] D. A. Pisner and D. M. Schnyer, "Support vector machine," in *Machine Learning*, A. Mechelli and S. Vieira, Eds. Oxford, UK: Academic Press, 2020, pp. 101–121, doi: 10.1016/B978-0-12-815739-8.00006-7.

[12] S. Sehgal *et al.*, "Unleashing potential and optimizing adolescent roller skating performance through a structured exercise program – a randomized controlled trial," *BMC Sports Sci. Med. Rehabil.*, vol. 15, no. 1, sep. 2023, doi: 10.1186/s13102-023-00728-x.

[13] G. J. van Ingen Schenau, R. W. De Boer, and G. De Groot, "Biomechanics of speed skating," in *Biomechanics of Sport*, C. L. Vaughan, Ed. Boca Raton, FL, USA: CRC Press, 2020, pp. 121–167, doi: 10.4324/9781003068549-4

[14] G. Bongiorno, F. G. Minisini, H. Biancuzzi, F. Dal Mas, and L. Miceli, "Skating efficiency and technique during roller speed skate using innovative piezoelectric smart socks : an exploratory study," *Front. Sports Act. Living*, vol. 7, pp. 1–10, jul. 2025, doi: 10.3389/fspor.2025.1554264.

[15] Z. Liu, M. Ding, M. Zhang, B. Yu, and H. Liu, "Effects of Technique Asymmetry on 500 m Speed Skating Performance," *Bioengineering*, vol. 11, no. 9, p. 899, sep. 2024, doi:

10.3390/bioengineering11090899.

[16] G. Bongiorno *et al.*, "The Kinematic and Electromyographic Analysis of Roller Skating at Different Speeds on a Treadmill : A Case Study," *Sensors*, vol. 24, no. 17, p. 5738, sep. 2024, doi: 10.3390/s24175738.

[17] Z. Cao, G. Hidalgo, T. Simon, S. E. Wei, and Y. Sheikh, "OpenPose: Realtime Multi-Person 2D Pose Estimation Using Part Affinity Fields," *IEEE Trans. Pattern Anal. Mach. Intell.*, vol. 43, no. 1, pp. 172–186, jan. 2021, doi: 10.1109/TPAMI.2019.2929257.

[18] C. Zheng *et al.*, "Deep Learning-based Human Pose Estimation : A Survey," *ACM Comput. Surv.*, vol. 56, no. 1, pp. 1–37, aug. 2023, doi: 10.1145/3603618.

[19] W. Hsu *et al.*, "PoseShot : hybrid CNN – BiLSTM transformer model for free throw action recognition via pose analysis," *Sci Rep*, vol. 16, no. 1, mar. 2026, doi: 10.1038/s41598-026-41025-0..

[20] S. C. Bakchy, M. Islam, M. R. Mahmud, and F. Imran, "Human Gait Analysis using Gait Energy Image," 2022, arXiv. doi: 10.48550/ARXIV.2203.09549.

[21] J. Loureiro and P. Lobato Correia, "Using a Skeleton Gait Energy Image for Pathological Gait Classification," in *Proc. 15th IEEE Int. Conf. Autom. Face Gesture Recognition* (FG 2020). IEEE, pp. 503–507, nov. 2020. doi: 10.1109/fg47880.2020.00064.

[22] P. Lee, T. Chen, H. Lin, L. Yeh, C. Liu, and Y. Chen, "Integrating OpenPose and SVM for Quantitative Postural Analysis in Young Adults : A Temporal-Spatial Approach," *Bioengineering*, vol. 11, no. 6, p. 548, may 2024, doi: 10.3390/bioengineering11060548.

[23] Z. Liu, M. Yang, K. Li, and X. Qin, "Recognition of TaeKwonDo kicking techniques based on accelerometer sensors," *Heliyon*, vol. 10, no. 12, p. e32475, jun. 2024, doi: 10.1016/j.heliyon.2024.e32475.

[24] I-H. Chung, "Using break-even analysis to explore the cost and carbon reduction benefits of solar and wind energy integration in microgrids for convenience stores," *Heliyon*, vol. 10, no. 21, p. e39644, nov. 2024, doi: 10.1016/j.heliyon.2024.e39644.

[25] P. Jafarzadeh, P. Virjonen, P. Nevalainen, F. Farahnakian, and J. Heikkonen, "Pose Estimation of Hurdles Athletes using OpenPose," in *2021 International Conference on Electrical, Computer, Communications and Mechatronics Engineering (ICECCME)*. IEEE, pp. 1–6, oct. 07, 2021. doi: 10.1109/iceccme52200.2021.9591066.

[26] M. E. Özateş, A. Yaman, F. Salami, S. Campos, S. I. Wolf, and U. Schneider, "Identification and interpretation of gait analysis features and foot conditions by explainable AI," *Sci. Rep.*, vol. 14, no. 1, mar. 2024, doi: 10.1038/s41598-024-56656-4..

[27] J. Stenum, C. Rossi, and R. T. Roemmich, "Two-dimensional video-based analysis of human gait using pose estimation," *PLoS Comput Biol*, vol. 17, no. 4, p. e1008935, Apr. 2021, doi: 10.1371/journal.pcbi.1008935.

[28] R. Hu *et al.*, "Effective evaluation of HGcnMLP method for markerless 3D pose estimation of musculoskeletal diseases patients based on smartphone monocular video," *Front. Bioeng. Biotechnol.*, vol. 11, jan. 2024, doi: 10.3389/fbioe.2023.1335251.

[29] N. J. Cronin *et al.*, "Feasibility of OpenPose markerless motion analysis in a real athletics competition," *Front. Sports Act. Living*, vol. 5, jan. 2024, doi: 10.3389/fspor.2023.1298003.

[30] M. Mundt, "Bridging the lab-to-field gap using machine learning : a narrative review," *Sport. Biomech.*, vol. 24, no. 10, pp. 2779–2798, apr. 2023, doi: 10.1080/14763141.2023.2200749.

[31] A. Alzahrani and A. Ullah, "Advanced biomechanical analytics : Wearable technologies for precision health monitoring in sports performance," *Digital Health*, vol. 10, jan. 2024, doi: 10.1177/20552076241256745.

[32] D. R. Seshadri *et al.*, "Wearable Technology and Analytics as a Complementary Toolkit to Optimize Workload and to Reduce Injury Burden," *Front. Sports Act. Living*, vol. 2, jan. 2021, doi: 10.3389/fspor.2020.630576.

[33] A. A. Phatak, F. G. Wieland, K. Vempala, F. Volkmar, and D. Memmert, "Artificial Intelligence Based Body Sensor Network Framework — Narrative Review : Proposing an End - to - End Framework using Wearable Sensors, Real - Time Location Systems and Artificial Intelligence/Machine Learning Algorithms for Data Collection , Data Mining and Knowledge Discovery in Sports and Healthcare," *Sport. Med. - Open*, vol. 7, no. 79, oct. 2021, doi: 10.1186/s40798-021-00372-0.

[34] M. Souaifi *et al.*, "Artificial Intelligence in Sports Biomechanics : A Scoping Review on Wearable Technology, Motion Analysis, and Injury Prevention," *Bioengineering*, vol. 12, no. 8, p. 887, aug. 2025, doi: 10.3390/bioengineering12080887.

[35] E. E. Cust, A. J. Sweeting, K. Ball, and S. Robertson, "Machine and deep learning for sport-specific movement recognition: a systematic review of model development and performance," vol. 37, no. 5, pp. 568–600, oct. 2019, doi: 10.1080/02640414.2018.1521769.

[36] B. Van Hooren, N. Pecasse, K. Meijer, and J. M. N. Essers, "The accuracy of markerless motion capture combined with computer vision techniques for measuring running kinematics," *Scand J Med Sci Sport*, vol. 33, no. 6, pp. 966–978, feb. 2023, doi: 10.1111/sms.14319.

[37] L. Xiang, A. Wang, Y. Gu, L. Zhao, V. Shim, and J. Fernandez "Recent Machine Learning Progress in Lower Limb Running Biomechanics With Wearable Technology : A Systematic Review," *Front. Neurorobot*., vol. 16, jun. 2022, doi: 10.3389/fnbot.2022.913052.

[38] C. Dindorf *et al*., "From lab to field with machine learning – Bridging the gap for movement analysis in real-world environments: A commentary," *Curr. Issues Sport Sci.*, vol. 9, no. 4, p. 014, sep. 2024, doi: 10.36950/2024.4CISS014.

[39] T. Y. Wang, J. Cui, and Y. Fan, "A wearable-based sports health monitoring system using CNN and LSTM with self-attentions," *PLoS One*, vol. 18, no. 10, p. e0292012, oct. 2023, doi: 10.1371/journal.pone.0292012.